NeuroImage: Clinical 19 (2018) 497–506

Contents lists available at ScienceDirect

NeuroImage: Clinical

journal homepage: www.elsevier.com/locate/ynicl

Longitudinal structural gray matter and white matter MRI changes in presymptomatic progranulin mutation carriers

Christopher A. Olm[a,b], Corey T. McMillan[a], David J. Irwin[a,c], Vivianna M. Van Deerlin[c], Philip A. Cook[b], James C. Gee[b], Murray Grossman[a,*]

[a] Penn Frontotemporal Degeneration Center, Department of Neurology, University of Pennsylvania, Philadelphia, PA, United States
[b] Penn Image Computing and Science Laboratory, Department of Radiology, University of Pennsylvania, Philadelphia, PA, United States
[c] Center for Neurodegenerative Disease Research, Department of Pathology and Laboratory Medicine, University of Pennsylvania, Philadelphia, PA, United States

ARTICLE INFO

Keywords:
Frontotemporal lobar degeneration
Magnetic resonance imaging
Neuroimaging
Progranulin
Presymptomatic
Longitudinal

ABSTRACT

Introduction: Mutations in the progranulin (*GRN*) gene are a major source of inherited frontotemporal degeneration (FTD) spectrum disorders associated with TDP-43 proteinopathy. We use structural MRI to identify regions of baseline differences and longitudinal changes in gray matter (GM) and white matter (WM) in presymptomatic *GRN* mutation carriers (pGRN+) compared to young controls (yCTL).

Methods: Cognitively intact first-degree relatives of symptomatic GRN+ FTD patients with identified *GRN* mutations (pGRN+; $N = 11$, mean age = 41.4) and matched yCTL ($N = 11$, mean age = 53.6) were identified. They completed a MRI session with T1-weighted imaging to assess GM density (GMD) and diffusion-weighted imaging (DWI) to assess fractional anisotropy (FA). Participants completed a follow-up session with T1 and DWI imaging (pGRN+ mean interval 2.20 years; yCTL mean interval 3.27 years). Annualized changes of GMD and FA were also compared.

Results: Relative to yCTL, pGRN+ individuals displayed reduced GMD at baseline in bilateral orbitofrontal, insular, and anterior temporal cortices. pGRN+ also showed greater annualized GMD changes than yCTL at follow-up in right orbitofrontal and left occipital cortices. We also observed reduced FA at baseline in bilateral superior longitudinal fasciculus, left corticospinal tract, and frontal corpus callosum in pGRN+ relative to yCTL, and pGRN+ displayed greater annualized longitudinal FA change in right superior longitudinal fasciculus and frontal corpus callosum.

Conclusions: Longitudinal MRI provides evidence of progressive GM and WM changes in pGRN+ participants relative to yCTL. Structural MRI illustrates the natural history of presymptomatic GRN carriers, and may provide an endpoint during disease-modifying treatment trials for pGRN+ individuals at risk for FTD.

1. Introduction

Frontotemporal degeneration (FTD) is a progressive neurodegenerative condition that typically begins with behavioral or language problems (Seelaar et al., 2011). The disease primarily affects frontal and anterior temporal brain regions. Approximately 25% of FTD cases are inherited (Wood et al., 2013), and one of the most common familial causes of FTD is a mutation of the progranulin (*GRN*) gene (Baker et al., 2006; Cruts et al., 2006). *GRN* mutations are universally associated with TDP-43 pathology (Neumann et al., 2006) and thus carriers may be good candidates for disease-modifying treatment trials (Boxer and Boeve, 2007; Gass et al., 2012), particularly in presymptomatic mutation carriers where a successful trial may be preventive.

Widespread reductions in gray matter (GM) volume and thickness have previously been shown in symptomatic GRN carriers (GRN+) compared to controls in frontal and temporal regions typically compromised in FTD, as well as in regions less frequently implicated in FTD such as the parietal lobes and precuneus (Premi et al., 2014b; Rohrer et al., 2010; Whitwell et al., 2009, 2007). A longitudinal evaluation of GM atrophy showed more rapid changes across frontal, temporal,

Abbreviations: GRN, progranulin; pGRN+, presymptomatic progranulin mutation carriers; GRN+, symptomatic progranulin mutation carriers; yCTL, young healthy controls; eCTL, elderly healthy controls; FTD, frontotemporal degeneration; GM, gray matter; WM, white matter; GMD, gray matter density; FA, fractional anisotropy; DWI, diffusion-weighted imaging; RD, radial diffusivity; AD, axial diffusivity; MD, mean diffusivity; ROI, region of interest; BA, Brodmann area; SLF, superior longitudinal fasciculus; IFO, inferior fronto-occipital fasciculus; ILF, inferior longitudinal fasciculus; CST, corticospinal tract

* Corresponding author at: Hospital of the University of Pennsylvania, 3400 Spruce Street, 3 West Gates, Philadelphia, PA 19104, United States
E-mail address: mgrossma@pennmedicine.upenn.edu (M. Grossman).

https://doi.org/10.1016/j.nicl.2018.05.017
Received 15 August 2017; Received in revised form 29 March 2018; Accepted 13 May 2018
Available online 15 May 2018

parietal, and even occipital regions in GRN+ individuals than sporadic FTD patients (Whitwell et al., 2015). Voxelwise studies of white matter (WM) in GRN+ cases of FTD have been examined less frequently, but extensive involvement of WM association fibers has been documented compared to healthy controls (Rohrer et al., 2010).

Prior cross-sectional structural and functional MRI imaging studies in presymptomatic *GRN* carriers (pGRN+) have identified differences in both GM and WM frontal and temporal regions (Borroni et al., 2012; Dopper et al., 2013; Pievani et al., 2014; Premi et al., 2014a). Yet, it remains to be shown that these changes are related to neurodegeneration rather than normal aging. Longitudinal studies looking at functional imaging have provided some evidence of presymptomic changes occurring in pGRN+ individuals in frontal, temporal, and parietal regions (Caroppo et al., 2015; Dopper et al., 2016). Changes observed in a longitudinal structural imaging study would provide some evidence that progression is due to neurodegeneration; one study has reported progressive atrophy in a temporal region in pGRN+ individuals (Caroppo et al., 2015), but this change was not compared to controls. Here, we provide novel evidence for longitudinal changes in brain structure derived from serial MRI imaging of pGRN+ individuals relative to controls. We hypothesized neurodegeneration in both GM and WM in pGRN+ at baseline, and greater annualized longitudinal changes relative to controls.

2. Materials and methods

2.1. Subjects

We identified symptomatic individuals with a *GRN* mutation (GRN+) from the Penn Frontotemporal Degeneration Center and Cognitive Neurology Clinic at the University of Pennsylvania ($N = 15$, 10 females) to be used as a symptomatic reference cohort for the pGRN+ comparisons. A board-certified neurologist with expertise in neurodegenerative conditions diagnosed these probands with an FTD-spectrum disease using published criteria (Gorno-Tempini et al., 2011; Rascovsky et al., 2011). The GRN+ cohort included different clinical presentations, including behavioral variant FTD (bvFTD; $N = 6$), corticobasal syndrome ($N = 4$), non-fluent/agrammatic primary progressive aphasia ($N = 3$), semantic variant primary progressive aphasia ($N = 1$), and Alzheimer's Disease ($N = 1$). To be included in this study, GRN+ patients had to have a T1-weighted MRI to assess GM density (GMD). A subset of these patients ($N = 9$, 5 females) also underwent a 30-directional diffusion-weighted imaging (DWI) sequence to assess fractional anisotropy (FA). A matched elderly healthy control group (eCTL; $N = 24$, 15 females) also underwent T1-weighted and 30-directional DWI MRI, though one was removed from the DWI analysis due to poor image quality due to artifact. Table 1 summarizes GRN+ and eCTL demographic information.

Table 1
Demographic characteristics of symptomatic progranulin mutation carriers (GRN+) and elderly controls (eCTL). The table displays the mean (standard deviation) of GRN+ and eCTL. Significant differences between GRN+ and eCTL are noted by * (two-sample *t*-tests, significance at $p < 0.05$).

	eCTL	GRN+
Number (female)	23 (15)	15 (10)
Age (years)	63.8 (7.37)	63.0 (6.62)
Education (years)	14.9 (2.26)	14.7 (3.83)
Symptomatic Disease Duration (years)	–	2.00 (1.07)
MMSE (max score = 30)*	29.2 (0.89)	19.0 (5.97)
Forward Digit Span*	7.40 (0.70)	5.67 (1.73)
Reverse Digit Span*	5.93 (1.10)	1.89 (1.62)
Boston Naming (max score = 30)*	28.2 (1.20)	17.4 (7.04)

Notes
1. Forward and reverse digit span and Boston naming test available for 9 GRN+.

First degree relatives of patients FTD were also recruited for research. These individuals were invited to participate in research that included MRI, neuropsychological testing, and genetic testing. For inclusion in the study, all of these individuals had to be cognitively normal, defined as no self-report of cognitive impairment and no reports of cognitive impairments by friends or family members, with a Clinical Dementia Rating (CDR) score of 0, and must have completed two MRI sessions that included a high resolution T1-weighted scan and a 30-directional DWI sequence. 11 individuals (7 females) that were first-degree relatives of symptomatic GRN+ patients had a mutation in *GRN* (pGRN+). We also recruited a matched young control group from the general population (yCTL; $N = 11$, 7 females). Subsets of the pGRN+ ($N = 1$) and yCTL ($N = 2$) had artifacts in their follow-up DWI scans and were thus excluded from the longitudinal WM analyses. No significant differences were found between pGRN+ and yCTL participants in demographic features, which included education, age, sex, or duration between scans (all $p > 0.05$). Also, no differences were found between pGRN+ and yCTL in baseline or follow-up neuropsychological testing performance (all $p > 0.05$), indicating that these individuals were truly without any evidence of disease. Table 2 summarizes demographic information and cognitive performance for presymptomatic cases. All participants completed a written informed consent procedure under a protocol approved by the Institutional Review Board convened at the University of Pennsylvania.

2.2. Genetic screening

DNA was extracted from peripheral blood following the manufacturer's protocols (Flexigene (Qiagen) or QuickGene DNA whole blood kit (Autogen)). Samples were tested for mutations in the entire *GRN* coding region using Sanger sequencing and/or targeted next generation sequencing (NGS) with a neurodegenerative disease-focused panel (multi neurodegenerative disease sequencing panel, MiND-Seq), that also tests for additional genes associated with FTD including *MAPT*, *VCP*, *CSF1R*, *TBK1*, *CHMP2B*, and *SQSTM1* (*C9orf72* expansion analysis was done separately) (Toledo et al., 2014; Wood et al., 2013). Sanger sequencing data were analyzed with Mutation Surveyor software (SoftGenetics, State College, PA) and alignment of sequence reads and variant calling from NGS were assessed by SureCall software (Agilent, Santa Clara, CA). Genetic screening revealed **11** asymptomatic participants with longitudinal MRI and a known pathogenic mutation of *GRN* associated with FTLD-TDP (Baker et al., 2006).

2.3. Image acquisition

All participants underwent a structural T1-weighted MPRAGE MRI acquired from a SIEMENS 3.0 T Trio scanner with an eight-channel coil using the following parameters: TR = 1620 ms; TE = 3 ms; 160 1.0 mm slices; flip angle = 15°; matrix = 192 × 256; in-plane resolution = 0.9766 mm × 0.9766 mm. In each session, all pGRN+ and yCTL participants also underwent a 30-directional DWI sequence, acquired using a single-shot, spin-echo, diffusion-weighted echo-planar imaging sequence with GRAPPA acceleration factor of 3. A subset of GRN+ patients were unable or unwilling to participate in the DWI portion of the protocol ($N = 6$). The diffusion sampling scheme consisted of either one or five images with $b = 0\ s/mm^2$, followed by measurements with 30 non-collinear/non-coplanar directions isotropically distributed in angular space ($b = 1000\ s/mm^2$), TR = 6700 ms, TE = 85 ms, slice thickness = 2.2 mm, and FOV 245 × 245 mm, reconstructed to 2.19 × 2.19 mm in-plane resolution.

2.4. Image preprocessing

2.4.1. Cross-sectional and baseline processing

To identify regions likely related to clinical disease and help validate our observations of MRI change in presymptomatic individuals, we

Table 2
Demographic Characteristics. The table displays the mean (standard deviation) of presymptomatic progranulin mutation carriers (pGRN+) and young controls (yCTL). There are no significant differences between pGRN+ and yCTL at baseline or follow-up (two sample t-tests, all $p > 0.05$).

	Baseline		Follow-up	
	pGRN+	yCTL	pGRN+	yCTL
Number (female)	11 (7)	11 (7)	11 (7)	11 (7)
Age	41.4 (13.4)	53.6 (15.0)	44.7 (13.0)	55.7 (15.2)
Education	16.7 (2.37)	15.9 (2.47)	16.7 (2.37)	15.9 (2.47)
Inter-scan interval	–	–	3.27 (2.02)	2.20 (1.42)
MMSE (max score = 30)	28.6 (1.71)	29.3 (1.16)	29.4 (1.03)	29.1 (1.05)
Forward digit span	7.70 (0.95)	7.43 (0.79)	7.70 (0.76)	7.67 (0.52)
Reverse digit span	6.30 (0.95)	5.86 (1.07)	6.55 (0.82)	5.71 (1.25)
Animal category fluency (words per minute)	24.5 (5.02)	20.4 (6.82)	27.7 (5.85)	21.9 (5.87)
Vegetable category fluency (words per minute)	17.9 (3.98)	15.6 (2.39)	20.9 (3.69)	17.0 (4.77)
Trails B time (seconds)	61.8 (24.4)	55.7 (25.9)	48.0 (13.7)	52.9 (17.3)
Trails B lines correct (max score = 24)	23.9 (0.25)	23.9 (0.24)	24.0 (0.00)	24.0 (0.00)
Boston naming (max score = 30)	28.8 (1.48)	28.1 (1.58)	29.3 (1.49)	29.1 (1.36)

Notes
1. 2 yCTL abstained from all cognitive testing, and an additional 2 individuals (1 pGRN+ and 1 yCTL) abstained from baseline cognitive testing.
2. In additional to those listed in 1., 3 yCTL and 2 pGRN+ did not have available follow-up fluency tests.
3. In additional to those listed in 1., 1 yCTL did not have available digit span tests and 1 pGRN+ did not have available baseline digit span tests.

examined changes in symptomatic GRN+ patients compared to elderly controls. We used a validated cross-sectional implementation of antsCorticalThickness, based on state-of-the-art ANTs (Tustison et al., 2014) to process T1-weighted images of GRN+ and eCTL individuals using the Penn Neurodegenerative Disease Template as our processing template. Each image was first bias-corrected for intensity inhomogeneity (Tustison et al., 2010) and was then deformed into the local template space in a canonical stereotactic coordinate system using a diffeomorphic deformation that is symmetric to minimize bias toward the reference space for computing the mappings and topology-preserving to capture the large deformation necessary to aggregate images in a common space. The ANTs Atropos expectation maximization algorithm (Avants et al., 2011) uses template-based priors to segment images into 6 tissue classes (cortical GM, subcortical GM, WM, CSF, brainstem, and cerebellum). Cortical GM probability images, a proxy for GMD, were then transformed into MNI152 space for analysis, using the convolution of the native-to-template and template-to-MNI152 transformations to minimize interpolation artifacts. The GMD images were then downsampled to 2 mm isotropic voxels and smoothed using a 4 mm isotropic full-width half-maximum kernel for analysis (equivalent to 2 voxels).

Diffusion tensors were calculated using a weighted linear least squares algorithm (Salvador et al., 2005) implemented in Camino (Cook et al., 2006). A regularized intra-scan session registration corrected for distortion between an individual's diffusion image and T1 image, which is composed with the warps between the T1 image, the group template, and MNI152 template. The anatomical alignment of diffusion tensors was then restored by applying the Preservation of Principal Directions algorithm (Alexander et al., 2001). Finally, FA was calculated in each voxel and then smoothed with a 2 mm isotropic full-width half-maximum kernel for analysis (equivalent to 2 voxels). Similarly, radial diffusivity (RD), axial diffusivity (AD), and mean diffusivity (MD) measures of WM integrity were calculated.

2.4.2. Longitudinal processing

Baseline and follow-up MRI volumes of the pGRN+ and yCTL individuals were preprocessed using ANTs, implemented using the antsLongitudinalCorticalThickness tool based on antsCorticalThickness (Tustison et al., 2014). Similar to cross-sectional processing, each image was first bias-corrected for intensity inhomogeneity (Tustison et al., 2010). Then, each pair of T1 scans was used to create a single subject template (SST) that is unbiased toward either scan. Segmentation of the SST was performed using antsMalfLabeling (Wang et al., 2013), which generates cortical GM, WM, subcortical GM, CSF, cerebellum, and brainstem probability images. These labeling priors were a subset of labeled datasets available from the Open Access Series of Imaging Studies (OASIS) (Marcus et al., 2007). antsCorticalThickness was performed on each timepoint using the SST segmentations as probability priors for the Atropos algorithm (Avants et al., 2011), which generated probability images for each of the 6 tissues mentioned above. The output cortical GM probability images were again used as a proxy of GMD. We smoothed the GMD images using a 4 mm isotropic full-width half maximum kernel, resampled to 2 mm isotropic voxels, then normalized to MNI152 space for analysis.

Similar to the cross-sectional pipeline for DWI, diffusion tensors were calculated using a weighted linear least squares algorithm (Salvador et al., 2005) implemented in Camino (Cook et al., 2006). A regularized intra-scan session registration corrects for distortion between an individual's diffusion image and T1 image, which is then composed with the warps between the T1 image, the SST, the group template, and MNI152 space. The anatomical alignment of diffusion tensors was then restored by applying the Preservation of Principal Directions algorithm (Alexander et al., 2001). Finally, FA was calculated in each voxel and then smoothed with a 2 mm isotropic full-width half maximum kernel.

Because we were interested in evaluating longitudinal changes, GMD and FA difference images were created by subtracting follow-up images from the respective baseline images. Then, difference images were normalized by dividing by the interscan interval to create annualized difference images (Caroppo et al., 2015; Olm et al., 2016).

2.5. Statistical analysis

2.5.1. Voxel-wise comparisons

We identified GM regions affected in GRN+ individuals relative to eCTL by performing voxel-wise *t*-tests of GMD, and similarly evaluated WM using FA. We also identified GM and WM regions where pGRN+ displayed baseline signs of neurodegeneration relative to yCTL by performing the respective voxel-wise t-tests of baseline GMD and FA. To identify regions of longitudinal change in GM and WM of pGRN+, we compared annualized difference images of GMD and FA, respectively, relative to yCTL. The Brodmann area (BA) of voxels of peak significance in GM are identified using the corresponding label from the Mindboggle-101 dataset (Klein and Tourville, 2012), and the tract associated with voxels of peak significance in FA analyses are identified using the ICBM-DTI-81 white-matter label atlas (Mori et al., 2008), each with verification by visual inspection of peak statistical voxels displayed on the MNI152 template (see results, below). For all

comparisons, we used the randomise tool in FSL to calculate non-parametric statistics (permutations = 10,000), as non-parametric tests require fewer assumptions about the distribution of the data and produce fewer false-positive results than parametric models (Winkler et al., 2014). All GM comparisons were constrained to regions with a cortical GM probability of > 0.35, and all WM comparisons restricted to within regions with a group mean FA > 0.20. Because age was trending toward being significantly different between pGRN+ and yCTL groups ($p = 0.06$), age at baseline MRI was used as a covariate for baseline and longitudinal comparisons of both GMD and FA. No GMD or FA baseline or longitudinal pGRN+ and yCTL contrasts reached significance after stringent correction for multiple comparisons, so more liberal, uncorrected thresholds were used. All comparisons were considered significant at $p < 0.01$ (uncorrected) with a cluster extent $> 500\,mm^3$. The reverse contrasts, looking for apparent reductions of both baseline and longitudinal GMD and FA in yCTL relative to pGRN+ were also examined. Voxel-wise AD, MD, and RD were also used to probe for signs of reduced WM integrity in pGRN+ relative to yCTL.

2.5.2. Lobe ROI comparisons

We also found the mean GMD in each of 12 brain lobes: frontal, insula, temporal, parietal, limbic, and occipital for each hemisphere for each GRN+ and eCTL participant. Then, using two-sample *t*-tests we compared lobe-wise measurements of GMD. Similar analyses were performed to compare baseline mean GMD between pGRN+ and yCTL, as well as mean annual change in GMD between pGRN+ and yCTL across each lobe. Differences for all contrasts were considered significant at $p < 0.05$.

3. Results

3.1. Symptomatic GM comparisons

We found widespread reduction in GMD in GRN+ relative to eCTL following an average of only two years of symptomatic disease. Fig. 1A (yellow) shows reduced GMD encompassing most of the bilateral frontal and temporal lobes, extending into the parietal lobes, as well as into the posterior cingulate, precuneus, and the occipital lobe. Peak voxel coordinates and other statistics are summarized in Table 3.

3.2. Baseline Presymptomatic GM comparisons

We found reduced baseline GMD in pGRN+ relative to yCTL. Fig. 2A (red) shows reduced GMD in pGRN+ in right orbitofrontal cortex (BA 11), extending into right anterior insula, as well as in right temporal pole (BA 38). Peak voxel coordinates and t-statistics are summarized in Table 4. No region displayed reduced GMD in yCTL relative to pGRN+.

3.3. Longitudinal Presymptomatic GM comparisons

Fig. 2A (orange) also illustrates greater annual changes in GMD in pGRN+ participants compared to yCTL. These regions included right orbitofrontal cortex (BA 10). We also observed longitudinal GMD change relative to controls in left occipital cortex (BA 18). Peak voxel coordinates and t-statistics are summarized in Table 5. No region displayed greater longitudinal GMD change in yCTL relative to pGRN+.

3.4. Symptomatic WM comparisons

GRN+ displayed widespread reductions in WM integrity measured using FA, as shown in Fig. 1B (green). Indications of WM damage appeared in most major association tracts, including superior longitudinal fasciculus (SLF), corticospinal tract (CST), inferior longitudinal fasciculus (ILF), inferior fronto-occipital fasciculus (IFO), cingulum, corpus callosum, and uncinate fasciculus, and extensively in frontal, temporal, and parietal subcortical WM; to a lesser extent, there is also reduced FA in subcortical occipital WM. For a summary of peak voxel coordinates and statistics, refer to Table 3. Similar results were found upon analysis of AD, RD, and MD. Please refer to supplemental Table e1 for the results of the RD, AD, and MD comparisons.

3.5. Baseline Presymptomatic WM comparisons

At baseline, pGRN+ displayed reduced FA in left SLF, right frontal corpus callosum, left IFO, and bilateral CST, shown in Fig. 2B (blue). Table 4 summarizes peak voxel coordinates and t-statistics. No region displayed reduced FA in yCTL relative to pGRN+, and there were no significant results at baseline in our pGRN+ > yCTL comparisons of AD, MD, or RD.

3.6. Longitudinal WM comparisons

pGRN+ participants displayed greater annualized FA changes than yCTL in right SLF and right frontal corpus callosum shown in Fig. 2B (cyan). Peak voxel coordinates and t-statistics are summarized in Table 5. No region displayed greater longitudinal FA change in yCTL than pGRN+. Longitudinal AD, MD, and RD were largely consistent with longitudinal FA results, all showing larger/additional clusters in the right SLF and frontal corpus callosum, and additionally showing results in bilateral CST, splenium of corpus callosum, right IFO and ILF, as well as left frontal corpus callosum. Please refer to supplemental Table e3 for the results of the RD, AD, and MD comparisons.

3.7. Lobe ROI comparisons

GRN+ displayed reduced mean GMD relative to eCTL in frontal, insula, temporal, parietal, and limbic ROIs for both the left and right hemispheres. There were no significant differences in mean GMD between pGRN+ and yCTL at baseline or in the annual change comparisons. For a summary of lobe ROI comparisons please refer to Table 6.

4. Discussion

Our results provide convincing evidence of progressive change in brain structures in presymptomatic individuals carrying a *GRN* mutation in comparison to healthy controls. We found that structural MRI detects reduced GM and WM integrity in pGRN+ individuals relative to yCTL at baseline, and furthermore that longitudinal structural MRI identifies both GM and WM regions showing greater annual changes in pGRN+ than yCTL. These areas overlap with GM and WM regions showing disease in symptomatic *GRN* mutation carriers, and thus our observations are consistent with the claim that pGRN+ have structural disease that eventually spreads more widely in the cerebrum to the point where symptomatic disease becomes apparent.

Past studies of symptomatic GRN+ individuals have consistently found widespread indications of both GM and WM alterations likely related to neurodegeneration (Premi et al., 2014b; Rohrer et al., 2010; Whitwell et al., 2015, 2009, 2007). Our results largely corroborate these past claims, showing fronto-temporal reductions in GMD typical of those found in FTD-spectrum disorders, with the noted additional involvement in parietal, posterior cingulate, precuneus, and occipital GM previously found in symptomatic GRN+ cohorts. Furthermore, the WM disease suggested by decreased FA in GRN+ relative to eCTL adds to prior work by showing extensive bilateral involvement at the group level in a voxel-wise analysis (Caroppo et al., 2014; Rohrer et al., 2010).

Consider in this context the baseline and longitudinal evaluations of structural MRI in presymptomatic *GRN* mutation carriers. We found reduced GMD in insula at baseline in pGRN+ individuals relative to yCTL. Cross-sectional imaging of pGRN+ individuals (Borroni et al., 2012) and pathological staging studies of patients with bvFTD due to TDP-43 pathology (Brettschneider et al., 2014) have suggested this as a

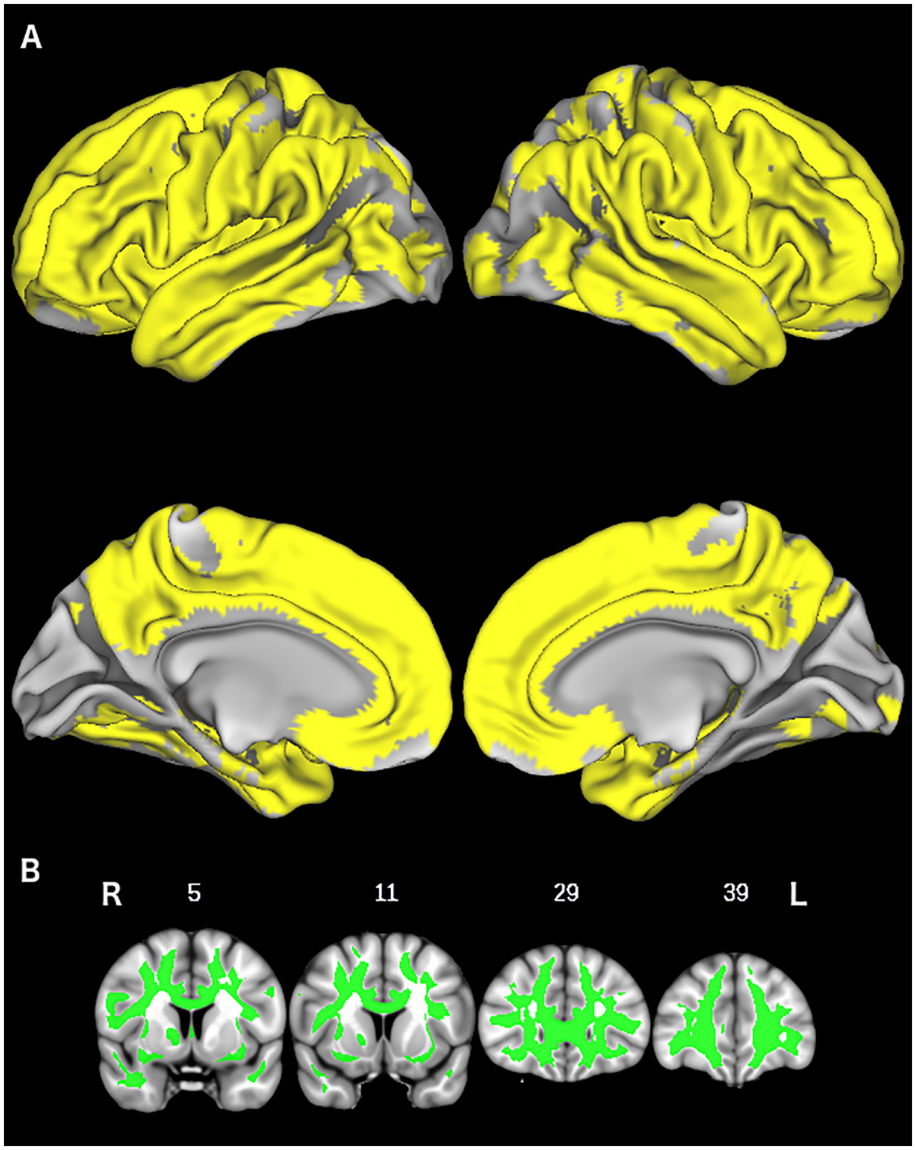

Fig. 1. Symptomatic progranulin mutation carriers (GRN+) compared to elderly controls (eCTL) A. GRN+ have reduced gray matter density (GMD) relative to eCTL, shown in yellow ($p < 0.01$ with a minimum cluster extent of 500 mm^3). B. GRN+ show widespread reduced fractional anisotropy (FA) relative to eCTL (green) ($p < 0.01$ with a cluster extent of 500 mm^3). (For interpretation of the references to color in this figure legend, the reader is referred to the web version of this article.)

Table 3
Statistical peaks of regions where symptomatic progranulin mutation carriers (GRN+) show differences relative to elderly controls (eCTL). Results summarized are those found in voxel-wise GMD image comparisons and voxel-wise fractional anisotropy (FA) image comparisons.

Anatomic locus	MNI coordinates			T-statistic	Cluster size
(Brodmann area)	X	Y	Z		(mm^3)
GMD differences					
L inferior frontal (45)	−40	12	6	10.6	589,424
R occipital (18)	26	−96	−6	4.50	2781
R fusiform (37)	36	−60	−14	4.71	1000
R occipital (18)	16	−76	−8	4.47	864
R occipital (19)	18	−86	28	3.81	600
FA differences					
Corpus callosum (body)	−8	10	24	9.16	255,285
R cerebellar white matter	26	−49	−31	5.14	2250
L cerebellar white matter	−11	−55	−24	4.97	948
R corpus callosum (posterior)	26	−86	11	4.85	554

candidate region for disease onset in FTD. This is consistent with resting BOLD imaging studies of healthy adults (Seeley et al., 2007) and imaging studies of symptomatic sporadic patients with bvFTD (Seeley et al., 2008) implicating the insula as an area of early involvement in FTD. The middle frontal cortex was previously reported in a cross-sectional study of pGRN+ individuals (Pievani et al., 2014), albeit on the left. Additionally, right primary motor regions were also previously found (Pievani et al., 2014). These reported insula and frontal regions contain von Economo neurons (Fajardo et al., 2008; von Economo and Koskinas, 1929) hypothesized to be a potential epicenter for the onset of FTD pathology (Seeley et al., 2012).

However, we also found evidence for very early disease in baseline imaging of pGRN+ in orbitofrontal cortex, an area an autopsy series has suggested is affected in the earliest stages of disease in TDP-43 proteinopathies (Brettschneider et al., 2014). Furthermore, we showed reductions in baseline GMD in right temporal pole, an area previously associated with aging in a pGRN+ cohort (Moreno et al., 2013). Some studies have found no structural or metabolic differences in GM when comparing pGRN+ to yCTL (Caroppo et al., 2015; Moreno et al., 2013),

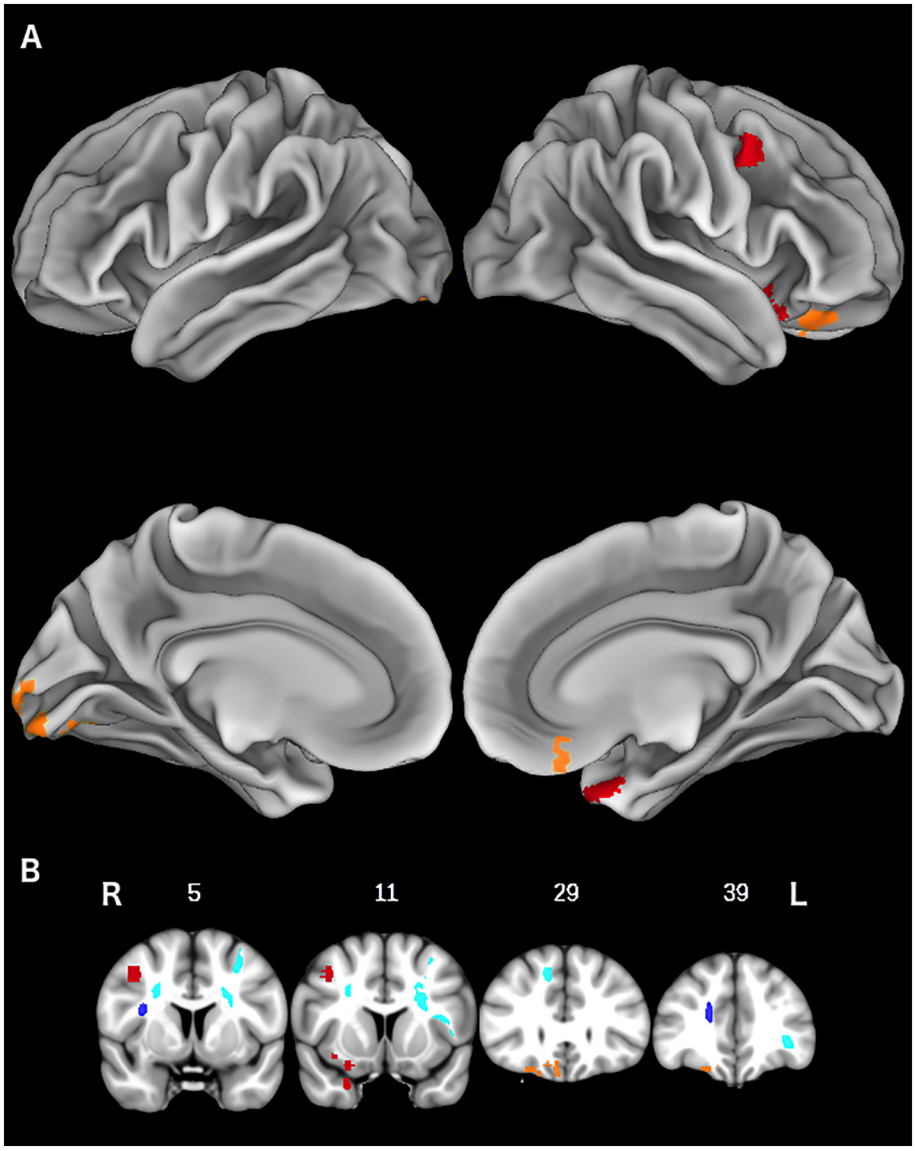

Fig. 2. Presymptomatic progranulin mutation carriers (pGRN+) compared to young controls (yCTL) A. pGRN+ have reduced gray matter density (GMD) at baseline (red) and greater annual GMD decreases (orange) relative to yCTL (results shown at $p < 0.01$ with a cluster extent of 500 mm^3). Note that pGRN+ displayed regions of both baseline and longitudinal GMD differences relative to yCTL. B. pGRN+ displayed reduced fractional anisotropy (FA) at baseline (blue) and greater annual FA decreases relative to yCTL (cyan) (results shown at $p < 0.01$ with a cluster extent of 500mm^3). (For interpretation of the references to color in this figure legend, the reader is referred to the web version of this article.)

raising the possibility that other genetic factors may influence eventual phenotype in these individuals (Finch et al., 2011). Indeed, recent image processing advances implemented here may have increased our sensitivity for detecting subtle differences in structural GM in these presymptomatic individuals (Tustison et al., 2014). It is nevertheless noteworthy that these temporal areas are not known to have von Economo neurons. This raises a question about the universal role of von Economo neurons in early FTD. The current study, and others assessing the earliest identifiable points in the course of FTD, is focused on carriers of a *GRN* mutation, and the onset of disease in a mutation carrier may differ from that of a sporadic case of FTD. Additional work is needed to help determine the epicenter (or epicenters) of sporadic and genetic forms of FTD.

We also observed greater longitudinal changes in GM in pGRN+ relative to yCTL. Right orbitofrontal GM regions displayed progressive change in pGRN+ relative to yCTL. These orbitofrontal areas are known to display longitudinal atrophy in populations of FTD patients, including those with GRN mutations (Whitwell et al., 2015). The orbitofrontal frontal cortex has also shown greater longitudinal change in functional PET imaging studies of pGRN+ relative to yCTL (Caroppo et al., 2015). Additionally, we found greater longitudinal change in left occipital cortex in pGRN+ relative to yCTL. A past report has linked all of these regions with aging in a pGRN+ cohort (Moreno et al., 2013). It is worth nothing that study also found an association between aging and additional frontotemporal regions, though this association was not compared with a control group leaving interpretation difficult (Moreno et al., 2013). Nearby occipital regions displayed reduced GMD in symptomatic GRN+ relative to eCTL in the present study, and were previously shown to exhibit progressive atrophy in symptomatic GRN+ relative to other mutation carriers and sporadic FTD cases, as well (Whitwell et al., 2015). Our observations cannot be easily attributed to healthy aging since our findings were significantly greater than longitudinal change found in a matched control cohort. Instead, we emphasize that progressive GM changes in presymptomatic cases are proximal to disease in symptomatic GRN+ cases. This suggests the possibility that these early progressive changes in pGRN+ represent a precursor to symptomatic disease as pathology continues to spread in these individuals. Additional longitudinal work in individuals converting from presymptomatic to symptomatic status is needed to assess this possibility.

One previous study demonstrated longitudinal cortical thickness change in a lateral temporal region in pGRN+ individuals that was not found here (Caroppo et al., 2015). However, the previous study included individuals who had converted to symptomatic status, whereas ours remained symptom-free and had neuropsychological testing at follow-up that was clearly within normal limits, and the study (Caroppo

Table 4
Regions where presymptomatic progranulin mutation carriers (pGRN+) show decreased gray matter density (GMD) and decreased fractional anisotropy (FA) at baseline relative to young controls (yCTL). Results summarized are those found in voxel-wise GMD image comparisons and voxel-wise FA image comparisons.

Anatomic locus	MNI coordinates			T-statistic	Cluster size
(Brodmann area)	X	Y	Z		(mm^3)
GMD differences					
R temporal pole (38)	26	14	−32	4.92	1144
R orbital (11)	26	12	−18	3.47	920
R middle frontal (9)	40	8	44	4.30	608
FA differences					
L superior longitudinal fasciculus/corticospinal tract	−23	12	27	6.37	2441
R corpus callosum (frontal)	9	32	45	5.97	636
L superior longitudinal fasciculus	−29	3	49	4.37	604
L superior longitudinal fasciculus	−38	8	14	3.56	567
R superior longitudinal fasciculus	26	8	36	3.96	508
L inferior fronto-occipital fasciculus	−29	45	4	4.33	500

Table 5
Regions where presymptomatic progranulin mutation carriers show greater annualized change than young controls. Results summarized are those found in voxel-wise gray matter density (GMD) annualized change image comparisons and voxel-wise fractional anisotropy (FA) annualized change image comparisons.

Anatomic locus	MNI Coordinates			T-statistic	Cluster size
(Brodmann area)	X	Y	Z		(mm^3)
GMD differences					
R orbital (11)	20	36	−22	3.66	672
R occipital (18)	−6	−94	−6	3.03	1112
R occipital (18)	−14	−80	−16	3.55	912
FA differences					
R superior longitudinal fasciculus	39	1	23	4.47	553
R corpus callosum (frontal)	18	41	18	4.65	541

et al., 2015) did not compare the longitudinal changes of pGRN+ to changes in a control group, thus not fully eliminating the possibility that the changes were related in part to normal aging. Moreover, studies of presymptomatic cases involve small cohorts of individuals, and some variability from study to study may be related in part to the underpowered nature of the imaging contrasts. Additional longitudinal work is needed in larger cohorts to determine the extent of progressive atrophy in pGRN+.

Observed differences in pGRN+ individuals at baseline were not restricted to GM, but also included differences in WM. We found reduced FA at baseline in IFO in pGRN+ relative to controls, similar to previous reports (Borroni et al., 2008; Dopper et al., 2013), and we additionally found reduced FA in left SLF and bilateral CST, similar to past work (Dopper et al., 2013; Pievani et al., 2014), as well as previously reported frontal projections of the corpus callosum (Dopper et al., 2013). More work will have to be done with larger cohorts and improved acquisition hardware and procedures to better determine the true course of WM damage in pGRN+. Additional cross-sectional studies have shown WM differences between pGRN+ relative to yCTL in uncinate (Borroni et al., 2008) and the cingulum (Pievani et al., 2014), though we note that we found longitudinal changes in the latter region. As with GM changes, we may not have observed these changes at baseline due to disease heterogeneity in an underpowered sample, and additional work is needed in larger samples to reliably establish the full extent of WM disease in pGRN+ individuals. We also observed longitudinal WM changes in the right SLF across all comparisons of WM disease. This area was previously shown to be affected in cross-sectional studies of pGRN+ individuals (Pievani et al., 2014), in GRN+ relative to carriers of other mutations (McMillan et al., 2014), and in GRN+ longitudinally relative to controls and MAPT+ (Rohrer et al., 2010), suggesting SLF may be specifically vulnerable early in individuals with a *GRN* mutation. AD, MD, and RD had somewhat more extensive longitudinal changes and no baseline differences, potentially suggesting that the different metrics calculated from DWI may be sensitive to somewhat different phases of the disease process (Song et al., 2002). Nevertheless, these WM regions, like the GM areas showing atrophy in the pGRN+ group, are encompassed by or partially overlapping the differences observed in symptomatic carriers relative to controls in this study. This lends support to the hypothesis that spreading disease in pGRN+ may surpass a threshold over time that eventually leads to the emergence of symptomatic disease.

Longitudinal studies such as ours may support speculation about the mechanisms underlying pathological disease progression that have been identified in animal models of neurodegenerative disease. Our results thus are not inconsistent with two different models of disease progression. The observed results in right orbitofrontal cortex, with reduced GM at baseline extending longitudinally to adjacent GM areas, may be consistent with a model of cell-to-cell, “prion-like,” spread that has been hypothesized in neurodegenerative disease, including in TDP-43 (Braak et al., 2014; Brettschneider et al., 2014; Clavaguera et al.,

Table 6
Comparisons of mean gray matter density (GMD) across each brain lobe between symptomatic progranulin mutation carriers (GRN+) and elderly controls (eCTL). Baseline GMD and annual change of GMD were also compared between presymptomatic progranulin mutation carriers (pGRN+) and young controls (yCTL). *Represents significant difference between GRN+ and eCTL at $p < 0.05$ using two-sample t-tests.

	Symptomatic			Presymptomatic baseline			Presymptomatic annual change		
Lobe	pValue	eCTL	GRN+	pValue	pGRN+	yCTL	pValue	pGRN+	yCTL
R limbic*	< 0.0001	0.5231	0.4739	0.4793	0.5480	0.5381	0.5708	−0.0045	−0.0059
L limbic*	< 0.0001	0.5153	0.4662	0.2203	0.5514	0.5335	0.5720	−0.0047	−0.0061
R insula*	< 0.0001	0.5292	0.4544	0.9248	0.5591	0.5574	0.4943	−0.0020	−0.0038
L insula*	< 0.0001	0.5252	0.4403	0.4673	0.5606	0.5473	0.4062	−0.0020	−0.0052
R frontal*	< 0.0001	0.4321	0.3496	0.4410	0.4741	0.4636	0.6353	−0.0054	−0.0043
L frontal*	< 0.0001	0.4307	0.3454	0.2052	0.4781	0.4602	0.6765	−0.0053	−0.0044
R parietal*	< 0.0001	0.4401	0.3874	0.2094	0.4838	0.4660	0.3796	−0.0053	−0.0030
L parietal*	< 0.0001	0.4402	0.3819	0.0894	0.4914	0.4661	0.3215	−0.0057	−0.0032
R occipital	0.1546	0.4433	0.4310	0.5157	0.5020	0.4945	0.2657	−0.0043	−0.0008
L occipital	0.1378	0.4373	0.4228	0.5119	0.4984	0.4911	0.1054	−0.0045	0.0001
R temporal*	0.0001	0.4901	0.4395	0.5066	0.5351	0.5276	0.4470	−0.0043	−0.0028
L temporal*	< 0.0001	0.4940	0.4347	0.2833	0.5345	0.5222	0.9693	−0.0041	−0.0040

2009; Walker and Jucker, 2015). We also found reduced baseline GMD in pGRN+ individuals in right middle frontal cortex, reduced FA at baseline in the adjacent SLF, and longitudinal changes in another nearby region in the right SLF at follow-up. This collection of results may fit another hypothesized "transneuronal" model of disease spread, by which disease begins in one cell and spreads to other cells through white matter projections (Seeley et al., 2009). Additional research, including longitudinal MRI studies with more timepoints and more sensitive T1-weighted and DWI acquisitions, is necessary to help determine the true pattern of pathological staging for pGRN+ individuals (Brettschneider et al., 2014; Irwin et al., 2016). Regardless of the underlying pathological mechanism, the longitudinal GM and WM changes shown here indicate that differences in pGRN+ relative to yCTL may be the result of progressive neurodegeneration and cannot be solely attributed to age-associated changes or developmental differences between pGRN+ and yCTL.

Strengths of our study include unique longitudinal observations of a clinically and quantitatively presymptomatic cohort using multimodal imaging. Longitudinal studies of symptomatic patients with likely FTLD-TDP pathology have demonstrated progressive disease using T1-weighted (Whitwell et al., 2015), DWI (Verstraete et al., 2014), and functional (Olm et al., 2016) imaging techniques, and appear to be consistent with models of spreading pathology, but we acknowledge a shortcoming of the current work is that it does not address pathological spreading directly. Though our pGRN+ and yCTL groups were matched demographically, the yCTL cohort did not consist of non-carrier relatives of pGRN+ so not all possible genetic factors are matched between groups. Since these individuals were presymptomatic, our selection of baseline was relatively arbitrary and does not account for variable age at penetrance (Rohrer et al., 2015). Penetrance of *GRN* mutations is thought to be reasonably high, around 90% by age 70 (Gass et al., 2006), and cognitive tests have not yet been discovered that are sensitive to the subtlest early clinical manifestations of disease. Our longitudinal model assumes a linear rate of disease progression throughout the preclinical phase of disease. Not all regions of reduced GM and WM in pGRN+ relative to yCTL at baseline also display greater longitudinal change. There is some difficulty in choosing appropriate statistical thresholds across imaging modalities; the authors attempted to assure that true effects are captured by choosing an appropriate threshold, that is not excessively liberal to capture false positives, while also not so conservative as to reject true positives. Though our results are not corrected for multiple comparisons and as such may be regarded with some skepticism, we maintain that our effort to show that there are no effects in the yCTL group relative to the pGRN+ group in GMD and FA comparisons indicate that our statistical thresholds were appropriately conservative. Lobe-wise analysis did not reveal differences between pGRN+ and yCTL, but the subtle, focal nature of disease onset revealed itself upon voxel-wise investigation. While our work shows progressive changes in both GM and WM in pGRN+ individuals, our findings may be confounded in part by mechanisms such as cognitive reserve (Massimo et al., 2015; Placek et al., 2016; Premi et al., 2013) that assist these individuals in maintaining their apparent presymptomatic status despite observed anatomic alterations. The sample size for our longitudinal evaluation of this rare mutation is small. However, our results and sample size are concordant with prior observations of individuals with *GRN* mutations (Borroni et al., 2012, 2008; Dopper et al., 2016; Pievani et al., 2014; Premi et al., 2014a; Whitwell et al., 2015), but additional work is needed with larger cohorts in an adequately powered study. Importantly, however, we observed no results indicating that yCTL have reduced GM or WM integrity relative to pGRN+ at baseline or longitudinally and thus we maintain that the presented findings are both significant and valid.

With these caveats in mind, we find pGRN+ appear to have significant neuroanatomic changes likely related to neurodegeneration prior to the emergence of clinical symptoms. Longitudinal structural MRI of both GM and WM provides evidence of progressive changes in pGRN+ individuals relative to yCTL in regions associated with disease in GRN+. Clinical trials may potentially benefit from structural MRI to monitor responses to disease-modifying treatments for pGRN+ at risk for developing FTD.

Acknowledgments

This work was supported by NIH Grants AG017586, AG032953, AG038490, AG043503, NS044266, NS053488, and NS088341, and the Dana Foundation, the Arking Family Foundation, and the Wyncote Foundation. No funding source had a role in the preparation, review, approval, or decision to submit the manuscript for publication.

Conflict of interest/disclosure statement

Conflicts of interest: none.

Appendix A. Supplementary data

Supplementary data to this article can be found online at https://doi.org/10.1016/j.nicl.2018.05.017.

References

Alexander, D.C., Pierpaoli, C., Basser, P.J., Gee, J.C., 2001. Spatial transformations of diffusion tensor magnetic resonance images. IEEE Trans. Med. Imaging 20, 1131–1139. http://dx.doi.org/10.1109/42.963816.

Avants, B.B., Tustison, N.J., Gee, J.C., 2011. An open source multivariate framework for n-tissue segmentation with evaluation on public data. Neuroinformatics 9, 381–400. http://dx.doi.org/10.1007/s12021-011-9109-y.An.

Baker, M., Mackenzie, I.R., Pickering-Brown, S.M., Gass, J., Rademakers, R., Lindholm, C., Snowden, J., Adamson, J., Sadovnick, A.D., Rollinson, S., Cannon, A., Dwosh, E., Neary, D., Melquist, S., Richardson, A., Dickson, D., Berger, Z., Eriksen, J., Robinson, T., Zehr, C., Dickey, C.A., Crook, R., McGowan, E., Mann, D., Boeve, B., Feldman, H., Hutton, M., 2006. Mutations in progranulin cause tau-negative frontotemporal dementia linked to chromosome 17. Nature 442, 916–919. http://dx.doi.org/10.1038/nature05016.

Borroni, B., Alberici, A., Premi, E., Archetti, S., Garibotto, V., Agosti, C., Gasparotti, R., Di Luca, M., Perani, D., Padovani, A., 2008. Brain magnetic resonance imaging structural changes in a pedigree of asymptomatic progranulin mutation carriers. Rejuvenation Res. 11, 585–595. http://dx.doi.org/10.1089/rej.2007.0623.

Borroni, B., Alberici, A., Cercignani, M., Premi, E., Serra, L., Cerini, C., Cosseddu, M., Pettenati, C., Turla, M., Archetti, S., Gasparotti, R., Caltagirone, C., Padovani, A., Bozzali, M., 2012. Granulin mutation drives brain damage and reorganization from preclinical to symptomatic FTLD. Neurobiol. Aging 33, 2506–2520. http://dx.doi.org/10.1016/j.neurobiolaging.2011.10.031.

Boxer, A.L., Boeve, B.F., 2007. Frontotemporal dementia treatment: current symptomatic therapies and implications of recent genetic, biochemical, and neuroimaging studies. Alzheimer Dis. Assoc. Disord. 21, S79–S87. http://dx.doi.org/10.1097/WAD.0b013e31815c345e.

Braak, H., Brettschneider, J., Ludolph, A.C., Lee, V.M., Trojanowski, J.Q., Del Tredici, K., 2014. Amyotrophic lateral sclerosis—a model of corticofugal axonal spread. Nat. Rev. Neurol. 9, 708–714. http://dx.doi.org/10.1038/nrneurol.2013.221.Amyotrophic.

Brettschneider, J., Del Tredici, K., Irwin, D.J., Grossman, M., Robinson, J.L., Toledo, J.B., Fang, L., Van Deerlin, V.M., Ludolph, A.C., Lee, V.M.Y., Braak, H., Trojanowski, J.Q., 2014. Sequential distribution of pTDP-43 pathology in behavioral variant frontotemporal dementia (bvFTD). Acta Neuropathol. 127, 423–439. http://dx.doi.org/10.1007/s00401-013-1238-y.

Caroppo, P., Le Ber, I., Camuzat, A., Clot, F., Naccache, L., Lamari, F., De Septenville, A., Bertrand, A., Belliard, S., Hannequin, D., Colliot, O., Brice, A., 2014. Extensive white matter involvement in patients with frontotemporal lobar degeneration. JAMA Neurol. 71, 1562. http://dx.doi.org/10.1001/jamaneurol.2014.1316.

Caroppo, P., Habert, M.O., Durrleman, S., Funkiewiez, A., Perlbarg, V., Hahn, V., Bertin, H., Gaubert, M., Routier, A., Hannequin, D., Deramecourt, V., Pasquier, F., Rivaud-Pechoux, S., Vercelletto, M., Edouart, G., Valabregue, R., Lejeune, P., Didic, M., Corvol, J.C., Benali, H., Lehericy, S., Dubois, B., Colliot, O., Brice, A., Le Ber, I., 2015. Lateral temporal lobe: an early imaging marker of the Presymptomatic GRN disease? J. Alzheimers Dis. 47, 751–759. http://dx.doi.org/10.3233/JAD-150270.

Clavaguera, F., Bolmont, T., Crowther, R.A., Abramowski, D., Frank, S., Probst, A., Fraser, G., Stalder, A.K., Beibel, M., Staufenbiel, M., Jucker, M., Goedert, M., Tolnay, M., 2009. Transmission and spreading of tauopathy in transgenic mouse brain. Nat. Cell Biol. 11, 909–913. http://dx.doi.org/10.1038/ncb1901.

Cook, P.A., Bai, Y., Seunarine, K.K., Hall, M.G., Parker, G.J., Alexander, D.C., 2006. Camino: open-source diffusion-MRI reconstruction and processing. Proc. Int. Soc. Magn. Reson. Med. 14, 2759.

Cruts, M., Gijselinck, I., van der Zee, J., Engelborghs, S., Wils, H., Pirici, D., Rademakers, R., Vandenberghe, R., Dermaut, B., Martin, J.J., van Duijn, C., Peeters, K., Sciot, R., Santens, P., De Pooter, T., Mattheijssens, M., Van den Broeck, M., Cuijt, I.,

Vennekens, K., De Deyn, P.P., Kumar-Singh, S., Van Broeckhoven, C., 2006. Null mutations in progranulin cause ubiquitin-positive frontotemporal dementia linked to chromosome 17q21. Nature 442, 920–924. http://dx.doi.org/10.1038/nature05017.

Dopper, E.G.P., Rombouts, S.A.R.B., Jiskoot, L.C., den Heijer, T., de Graaf, J.R.A., de Koning, I., Hammerschlag, A.R., Seelaar, H., Seeley, W.W., Veer, I.M., van Buchem, M.A., Rizzu, P., van Swieten, J.C., 2013. Structural and functional brain connectivity in presymptomatic familial frontotemporal dementia. Neurology 80, 814–823. http://dx.doi.org/10.1212/WNL.0b013e31828407bc.

Dopper, E.G.P., Chalos, V., Ghariq, E., den Heijer, T., Hafkemeijer, A., Jiskoot, L.C., de Koning, I., Seelaar, H., van Minkelen, R., van Osch, M.J.P., Rombouts, S.A.R.B., van Swieten, J.C., 2016. Cerebral blood flow in presymptomatic MAPT and GRN mutation carriers: a longitudinal arterial spin labeling study. NeuroImage Clin. 12, 460–465. http://dx.doi.org/10.1016/j.nicl.2016.08.001.

von Economo, C., Koskinas, G.N., 1929. The Cytoarchitectonics of the Human Cerebral Cortex. The Oxford University Press.

Fajardo, C., Escobar, M.I., Buriticá, E., Arteaga, G., Umbarila, J., Casanova, M.F., Pimienta, H., 2008. Von Economo neurons are present in the dorsolateral (dysgranular) prefrontal cortex of humans. Neurosci. Lett. 435, 215–218. http://dx.doi.org/10.1016/j.neulet.2008.02.048.

Finch, N., Carrasquillo, M.M., Rutherford, N.J., Coppola, G., DeJesus-Hernandez, M., Crook, R., Hunter, T., Ghidoni, R., Benussi, L., Crook, J., Finger, E., Hantanpaa, K.J., Karydas, A.M., Sengdy, P., Gonzalez, J., Seeley, W.W., Johnson, N., Beach, T.G., Mesulam, M., Forloni, G., Kertesz, A., Knopman, D.S., Uitti, R., White, C.L., Caselli, R., Lippa, C., Bigio, E.H., Wszolek, Z.K., Binetti, G., Mackenzie, I.R., Miller, B.L., Boeve, B.F., Younkin, S.G., Dickson, D.W., Petersen, R.C., Graff-Radford, N.R., Geschwind, D.H., Rademakers, R., 2011. TMEM106B regulates progranulin levels and the penetrance of FTLD in GRN mutation carriers. Neurology 75, 467–474.

Gass, J., Cannon, A., Mackenzie, I.R., Boeve, B., Baker, M., Adamson, J., Crook, R., Melquist, S., Kuntz, K., Petersen, R., Josephs, K., Pickering-Brown, S.M., Graff-Radford, N., Uitti, R., Dickson, D., Wszolek, Z., Gonzalez, J., Beach, T.G., Bigio, E., Johnson, N., Weintraub, S., Mesulam, M., White, C.L., Woodruff, B., Caselli, R., Hsiung, G.Y., Feldman, H., Knopman, D., Hutton, M., Rademakers, R., 2006. Mutations in progranulin are a major cause of ubiquitin-positive frontotemporal lobar degeneration. Hum. Mol. Genet. 15, 2988–3001. http://dx.doi.org/10.1093/hmg/ddl241.

Gass, J., Prudencio, M., Stetler, C., Petrucelli, L., 2012. Progranulin: an emerging target for FTLD therapies. Brain Res. 1462, 118–128. http://dx.doi.org/10.1016/j.brainres.2012.01.047.

Gorno-Tempini, M.L., Hillis, A.E., Weintraub, S., Kertesz, A., Mendez, M., Cappa, S.F., Ogar, J.M., Rohrer, J.D., Black, S., Boeve, B.F., Manes, F., Dronkers, N.F., Vandenberghe, R., Rascovsky, K., Patterson, K., Miller, B.L., Knopman, D.S., Hodges, J.R., Mesulam, M.M., Grossman, M., 2011. Classification of primary progressive aphasia and its variants. Neurology 76, 1006–1014. http://dx.doi.org/10.1212/WNL.0b013e31821103e6.

Irwin, D.J., Brettschneider, J., McMillan, C.T., Cooper, F., Olm, C., Arnold, S.E., Van Deerlin, V.M., Seeley, W.W., Miller, B.L., Lee, E.B., Lee, V.M.Y., Grossman, M., Trojanowski, J.Q., 2016. Deep clinical and neuropathological phenotyping of pick disease. Ann. Neurol. 79, 272–287. http://dx.doi.org/10.1002/ana.24559.

Klein, A., Tourville, J., 2012. 101 labeled brain images and a consistent human cortical labeling protocol. Front. Neurosci. 6, 171. http://dx.doi.org/10.3389/fnins.2012.00171.

Marcus, D.S., Fotenos, A.F., Csernansky, J.G., Morris, J.C., Buckner, R.L., 2007. Open access series of imaging studies (OASIS): cross-sectional MRI data in young, middle aged, nondemented and demented older adults. J. Cogn. Neurosci. 19, 1498–1507. http://dx.doi.org/10.1162/jocn.2007.19.9.1498.

Massimo, L., Zee, J., Xie, S.X., McMillan, C.T., Rascovsky, K., Irwin, D.J., Kolanowski, A., Grossman, M., 2015. Occupational attainment influences survival in autopsy-confirmed frontotemporal degeneration. Neurology 84, 2070–2075. http://dx.doi.org/10.1212/WNL.0000000000001595.

McMillan, C.T., Toledo, J.B., Avants, B.B., Cook, P.A., Wood, E.M., Suh, E., Irwin, D.J., Powers, J., Olm, C., Elman, L., McCluskey, L., Schellenberg, G.D., Lee, V.M.-Y., Trojanowski, J.Q., Van Deerlin, V.M., Grossman, M., 2014. Genetic and neuroanatomic associations in sporadic frontotemporal lobar degeneration. Neurobiol. Aging 35, 1473–1482. http://dx.doi.org/10.1016/j.neurobiolaging.2013.11.029.

Moreno, F., Sala-Llonch, R., Barandiaran, M., Sánchez-Valle, R., Estanga, A., Bartrés-Faz, D., Sistiaga, A., Alzualde, A., Fernández, E., Martí Massó, J.F., López de Munain, A., Indakoetxea, B., 2013. Distinctive age-related temporal cortical thinning in asymptomatic granulin gene mutation carriers. Neurobiol. Aging 34, 1462–1468. http://dx.doi.org/10.1016/j.neurobiolaging.2012.11.005.

Mori, S., Oishi, K., Jiang, H., Jiang, L., Li, X., Akhter, K., Hua, K., Faria, A.V., Mahmood, A., Woods, R., Toga, A., Pike, B., Rosa-Neto, P., Evans, A., Zhang, J., Huang, H., Miller, M.I., van Zijl, P., Mazziotta, J., 2008. Stereotaxic white matter atlas based on diffusion tensor imaging in an ICBM template. NeuroImage 40, 570–582.

Neumann, M., Sampathu, D.M., Kwong, L.K., Truax, A.C., Micsenyi, M.C., Chou, T.T., Bruce, J., Schuck, T., Grossman, M., Clark, C.M., McCluskey, L.F., Miller, B.L., Masliah, E., Mackenzie, I.R., Feldman, H., Feiden, W., Kretzschmar, H.A., Trojanowski, J.Q., Lee, V.M.-Y., 2006. Ubiquitinated TDP-43 in frontotemporal lobar degeneration and amyotrophic lateral sclerosis. Science 314 (80), 130–133. http://dx.doi.org/10.1126/science.1134108.

Olm, C.A., Kandel, B.M., Avants, B.B., Detre, J.A., Gee, J.C., Grossman, M., McMillan, C.T., 2016. Arterial spin labeling perfusion predicts longitudinal decline in semantic variant primary progressive aphasia. J. Neurol. 263, 1927–1938. http://dx.doi.org/10.1007/s00415-016-8221-1.

Pievani, M., Paternico, D., Benussi, L., Binetti, G., Orlandini, A., Cobelli, M., Magnaldi, S., Ghidoni, R., Frisoni, G.B., 2014. Pattern of structural and functional brain abnormalities in asymptomatic granulin mutation carriers. Alzheimers Dement. 10, S354–S363. http://dx.doi.org/10.1016/j.jalz.2013.09.009.

Placek, K., Massimo, L., Olm, C., Ternes, K., Firn, K., Van Deerlin, V., Lee, E.B., Trojanowski, J.Q., Lee, V.M.Y., Irwin, D., Grossman, M., McMillan, C.T., 2016. Cognitive reserve in frontotemporal degeneration. Neurology 87, 1813–1819. http://dx.doi.org/10.1212/WNL.0000000000003250.

Premi, E., Gazzina, S., Bozzali, M., Archetti, S., Alberici, A., Cercignani, M., Bianchetti, A., Gasparotti, R., Turla, M., Caltagirone, C., Padovani, A., Borroni, B., 2013. Cognitive reserve in Granulin-related frontotemporal dementia: from preclinical to clinical stages. PLoS One 8, 1–8. http://dx.doi.org/10.1371/journal.pone.0074762.

Premi, E., Cauda, F., Gasparotti, R., Diano, M., Archetti, S., Padovani, A., Borroni, B., 2014a. Multimodal fMRI resting-state functional connectivity in Granulin mutations: the case of fronto-parietal dementia. PLoS One 9. http://dx.doi.org/10.1371/journal.pone.0106500.

Premi, E., Garibotto, V., Gazzina, S., Formenti, A., Archetti, S., Gasparotti, R., Padovani, A., Borroni, B., 2014b. Subcortical and deep cortical atrophy in frontotemporal dementia due to Granulin mutations. Dement. Geriatr. Cogn. Dis. Extra 4, 95–102. http://dx.doi.org/10.1159/000355428.

Rascovsky, K., Hodges, J.R., Knopman, D., Mendez, M.F., Kramer, J.H., Neuhaus, J., Van Swieten, J.C., Seelaar, H., Dopper, E.G.P., Onyike, C.U., Hillis, A.E., Josephs, K.A., Boeve, B.F., Kertesz, A., Seeley, W.W., Rankin, K.P., Johnson, J.K., Gorno-Tempini, M.L., Rosen, H., Prioleau-Latham, C.E., Lee, A., Kipps, C.M., Lillo, P., Piguet, O., Rohrer, J.D., Rossor, M.N., Warren, J.D., Fox, N.C., Galasko, D., Salmon, D.P., Black, S.E., Mesulam, M., Weintraub, S., Dickerson, B.C., Diehl-Schmid, J., Pasquier, F., Deramecourt, V., Lebert, F., Pijnenburg, Y., Chow, T.W., Manes, F., Grafman, J., Cappa, S.F., Freedman, M., Grossman, M., Miller, B.L., 2011. Sensitivity of revised diagnostic criteria for the behavioural variant of frontotemporal dementia. Brain 134, 2456–2477. http://dx.doi.org/10.1093/brain/awr179.

Rohrer, J.D., Ridgway, G.R., Modat, M., Ourselin, S., Mead, S., Fox, N.C., Rossor, M.N., Warren, J.D., 2010. Distinct profiles of brain atrophy in frontotemporal lobar degeneration caused by progranulin and tau mutations. NeuroImage 53, 1070–1076. http://dx.doi.org/10.1016/j.neuroimage.2009.12.088.

Rohrer, J.D., Nicholas, J.M., Cash, D.M., van Swieten, J., Dopper, E., Jiskoot, L., van Minkelen, R., Rombouts, S.A., Cardoso, M.J., Clegg, S., Espak, M., Mead, S., Thomas, D.L., De Vita, E., Masellis, M., Black, S.E., Freedman, M., Keren, R., MacIntosh, B.J., Rogaeva, E., Tang-Wai, D., Tartaglia, M.C., Laforce, R., Tagliavini, F., Tiraboschi, P., Redaelli, V., Prioni, S., Grisoli, M., Borroni, B., Padovani, A., Galimberti, D., Scarpini, E., Arighi, A., Fumagalli, G., Rowe, J.B., Coyle-Gilchrist, I., Graff, C., Fallström, M., Jelic, V., Ståhlbom, A.K., Andersson, C., Thonberg, H., Lilius, L., Frisoni, G.B., Pievani, M., Bocchetta, M., Benussi, L., Ghidoni, R., Finger, E., Sorbi, S., Nacmias, B., Lombardi, G., Polito, C., Warren, J.D., Ourselin, S., Fox, N.C., Rossor, M.N., 2015. Presymptomatic cognitive and neuroanatomical changes in genetic frontotemporal dementia in the Genetic Frontotemporal dementia Initiative (GENFI) study: a cross-sectional analysis. Lancet Neurol. 14, 253–262. http://dx.doi.org/10.1016/S1474-4422(14)70324-2.

Salvador, R., Peña, A., Menon, D.K., Carpenter, T.A., Pickard, J.D., Bullmore, E.T., 2005. Formal characterization and extension of the linearized diffusion tensor model. Hum. Brain Mapp. 24, 144–155. http://dx.doi.org/10.1002/hbm.20076.

Seelaar, H., Rohrer, J.D., Pijnenburg, Y.A.L., Fox, N.C., van Swieten, J.C., 2011. Clinical, genetic and pathological heterogeneity of frontotemporal dementia: a review. J. Neurol. Neurosurg. Psychiatry 82, 476–486. http://dx.doi.org/10.1136/jnnp.2010.212225.

Seeley, W.W., Menon, V., Schatzberg, A.F., Keller, J., Glover, G.H., Kenna, H., Reiss, A.L., Greicius, M.D., 2007. Dissociable intrinsic connectivity networks for salience processing and executive control. J. Neurosci. 27, 2349–2356. http://dx.doi.org/10.1523/JNEUROSCI.5587-06.2007.

Seeley, W.W., Crawford, R., Rascovsky, K., Kramer, J.H., Weiner, M., Miller, B.L., Gorno-Tempini, M.L., 2008. Frontal paralimbic network atrophy in very mild behavioral variant frontotemporal dementia. Arch. Neurol. 65, 249–255. http://dx.doi.org/10.1001/archneurol.2007.38.

Seeley, W.W., Crawford, R.K., Zhou, J., Miller, B.L., Greicius, M.D., 2009. Neurodegenerative diseases target large-scale human brain networks. Neuron 62, 42–52. http://dx.doi.org/10.1016/j.neuron.2009.03.024.

Seeley, W.W., Merkle, F.T., Gaus, S.E., Craig, A.D., Allman, J.M., Hof, P.R., 2012. Distinctive neurons of the anterior cingulate and frontoinsular cortex: a historical perspective. Cereb. Cortex 22, 245–247. http://dx.doi.org/10.1093/cercor/bhr005.

Song, S.K., Sun, S.W., Ramsbottom, M.J., Chang, C., Russell, J., Cross, A.H., 2002. Dysmyelination revealed through MRI as increased radial (but unchanged axial) diffusion of water. NeuroImage 17, 1429–1436. http://dx.doi.org/10.1006/nimg.2002.1267.

Toledo, J.B., Van Deerlin, V.M., Lee, E.B., Suh, E., Baek, Y., Robinson, J.L., Xie, S.X., McBride, J., Wood, E.M., Schuck, T., Irwin, D.J., Gross, R.G., Hurtig, H., McCluskey, L., Elman, L., Karlawish, J., Schellenberg, G., Chen-Plotkin, A., Wolk, D., Grossman, M., Arnold, S.E., Shaw, L.M., Lee, V.M.-Y., Trojanowski, J.Q., 2014. A platform for discovery: the University of Pennsylvania Integrated Neurodegenerative Disease Biobank. Alzheimers Dement. 10, 447–484. http://dx.doi.org/10.1016/j.jalz.2013.06.003.

Tustison, N.J., Avants, B.B., Cook, P.A., Zheng, Y., Egan, A., Yushkevich, P.A., Gee, J.C., 2010. N4ITK: improved N3 bias correction. IEEE Trans. Med. Imaging 29, 1310–1320. http://dx.doi.org/10.1109/TMI.2010.2046908.

Tustison, N.J., Cook, P.A., Klein, A., Song, G., Das, S.R., Duda, J.T., Kandel, B.M., van Strien, N., Stone, J.R., Gee, J.C., Avants, B.B., 2014. Large-scale evaluation of ANTs and FreeSurfer cortical thickness measurements. NeuroImage 99, 166–179. http://dx.doi.org/10.1016/j.neuroimage.2014.05.044.

Verstraete, E., Veldink, J.H., van den Berg, L.H., van den Heuvel, M.P., 2014. Structural brain network imaging shows expanding disconnection of the motor system in amyotrophic lateral sclerosis. Hum. Brain Mapp. 35, 1351–1361. http://dx.doi.org/

10.1002/hbm.22258.
Walker, L.C., Jucker, M., 2015. Neurodegenerative diseases: expanding the prion concept. Annu. Rev. Neurosci. 38, 87–103. http://dx.doi.org/10.1146/annurev-neuro-071714-033828.
Wang, H., Suh, J.W., Das, S.R., Pluta, J., Craige, C., Yushkevich, P.A., 2013. Multi-atlas segmentation with joint label fusion. IEEE Trans. Pattern Anal. Mach. Intell. 35, 611–623. http://dx.doi.org/10.1109/TPAMI.2012.143.
Whitwell, J.L., Jack, C.R., Baker, M., Rademakers, R., Adamson, J., Boeve, B.F., Knopman, D.S., Parisi, J.F., Petersen, R.C., Dickson, D.W., Hutton, M.L., Josephs, K.A., 2007. Voxel-based morphometry in frontotemporal lobar degeneration with ubiquitin-positive inclusions with and without progranulin mutations. Arch. Neurol. 64, 371–376. http://dx.doi.org/10.1001/archneur.64.3.371.
Whitwell, J.L., Jack, C.R., Boeve, B.F., Senjem, M.L., Baker, M., Rademakers, R., Ivnik, R.J., Knopman, D.S., Wszolek, Z.K., Petersen, R.C., Josephs, K.A., 2009. Voxel-based morphometry patterns of atrophy in FTLD with mutations in MAPT or PGRN. Neurology 72, 813–820. http://dx.doi.org/10.1212/01.wnl.0000343851.46573.67.
Whitwell, J.L., Boeve, B.F., Weigand, S.D., Senjem, M.L., Gunter, J.L., Baker, M.C., DeJesus-Hernandez, M., Knopman, D.S., Wszolek, Z.K., Petersen, R.C., Rademakers, R., Jack, C.R., Josephs, K.A., 2015. Brain atrophy over time in genetic and sporadic frontotemporal dementia: a study of 198 serial magnetic resonance images. Eur. J. Neurol. 22, 745–752. https://doi.org/10.1111/ene.12675.
Winkler, A.M., Ridgway, G.R., Webster, M.A., Smith, S.M., Nichols, T.E., 2014. Permutation inference for the general linear model. NeuroImage 92, 381–397. http://dx.doi.org/10.1016/j.neuroimage.2014.01.060.
Wood, E.M., Falcone, D., Suh, E., Irwin, D.J., Alice, S., Lee, E.B., Xie, S.X., Van Deerlin, V.M., Grossman, M., 2013. Development and validation of pedigree classification criteria for frontotemporal lobar degeneration. J. Am. Med. Assoc. Neurol. 70, 1411–1417. http://dx.doi.org/10.1001/jamaneurol.2013.3956.Development.